Pauli blocking effects in $n\alpha$-nucleus-induced fusion reactions

Kaixuan Cheng and Chang Xu*
School of Physics, Nanjing University, Nanjing 210093, China

(Received 21 May 2020; accepted 13 July 2020; published 27 July 2020)

The hindrances in the $n\alpha$-nucleus-induced fusion reactions at deep subbarrier energies are investigated by using the coupled-channels model. Inspired by the microscopic Pauli-blocking effects of α-cluster decay in radioactive nuclei, a Pauli blocking potential is constructed in the $n\alpha$-nucleus-induced fusion reactions by using a single folding procedure, in which the $n\alpha$ nuclei are assumed to be consisted of α particles. A shallow pocket is formed in the inner part of the potential between two colliding nuclei as compared to the one obtained from the double-folding potential with standard Michigan-3-Yukawa effective nucleon-nucleon interaction. The experimental fusion cross sections are described well for fusion systems $^{12}C + ^{198}Pt$, $^{16}O + ^{208}Pb$, $^{12}C + ^{30}Si$, $^{24}Mg + ^{30}Si$, and $^{28}Si + ^{30}Si$. At deep subbarrier energies, it is found that this shallow pocket potential reduces the partial fusion cross sections and shields the contributions of high-angular-momentum partial waves to fusion cross sections. In addition, a detailed comparison of fusion processes with different projectiles ^{12}C, ^{24}Mg, and ^{28}Si on the same target ^{30}Si shows the hindrance effect is stronger for heavier projectiles.

DOI: 10.1103/PhysRevC.102.014619

I. INTRODUCTION

The fusion hindrance phenomenon observed recently at deep subbarrier energies in heavy-ion fusion reactions presents a new challenge to the current fusion theory [1]. This unexpected falloff feature in experimental fusion cross sections [1–8] is hard to explain by the standard coupled-channels (CC) model with the widely used Woods-Saxon (WS) potential, which has been successful in describing the enhancement of fusion cross sections at subbarrier energies [9,10]. By adjusting the diffuseness parameter in WS nuclear potential, the calculated fusion cross sections are found to be in agreement with the experimental data at deep subbarrier energies [11]. However, there is a large discrepancy between the diffuseness parameters used in WS potential $a \approx 1.3$ fm [11] and the one extracted from scattering data $a \approx 0.63$ fm [12]. This discrepancy implies that the Woods-Saxon nuclear potential is probably only valid in the surface region [13,14]. When the densities of projectile and target nuclei start overlapping, the effect of Pauli blocking interaction might become more and more important in the inner region of the Coulomb barrier.

In recent years, a number of theoretical work have been devoted to investigating the fusion hindrance at deep subbarrier energies [15–27]. For instance, based on the frozen density approximation, Mişicu and Esbensen introduced a strong repulsive core to the calculation of fusion reactions $^{64}Ni + ^{64}Ni$, etc., and the calculated fusion cross sections at deep subbarrier energies reproduce the experimental data very well [16–18]. Uegaki and Abe also proposed a strong repulsive potential to treat the density overlap problem, which is found to be necessary for the folding potential in describing the high-spin resonances observed in scattering reactions [28]. With the repulsive potential, the calculated resonance levels are in good agreement with experimental data [28]. Very recently, a preliminary work about the Pauli blocking effects in α-induced fusion reactions also provided a good description of the fusion cross sections for reactions $\alpha + ^{208}Pb$, etc. [29].

Until now, the hindrance phenomenon has been mainly observed in the fusion systems with heavy target [2,3]. What is interesting is whether this hindrance also occurs in light fusion systems [30,31]. In light nuclei, especially for $n\alpha$ nuclei ^{12}C, ^{16}O, ^{24}Mg, and ^{28}Si, it is a well-known fact that many states are of α cluster type and this description has enjoyed considerable success [32–36]. In this paper, based on the α-cluster structures in $n\alpha$ nuclei, the Pauli blocking effects in $n\alpha$-nucleus-induced fusion reactions are introduced to explain the fusion hindrance at deep subbarrier energies. By considering the Pauli blocking effects, the partial fusion cross sections at colliding energies far below the Coulomb barrier are analyzed. The comparison of total fusion cross sections is made between the experimental data and calculation results for $^{12}C + ^{30}Si$ [4], $^{12}C + ^{198}Pt$ [5], $^{16}O + ^{208}Pb$ [6], $^{24}Mg + ^{30}Si$ [7], and $^{28}Si + ^{30}Si$ [8] fusion systems. In addition, the Pauli blocking potentials between different projectiles and the same target, i.e., $^{12}C + ^{30}Si$, $^{24}Mg + ^{30}Si$, and $^{28}Si + ^{30}Si$ fusion systems, are employed to explore the fusion hindrance from light projectile to heavy one. The above analysis might be helpful not only in exploring the hindrance of the heavy-ion fusion reactions at deep subbarrier energies under laboratory conditions but also in understanding the fusion process of the light systems in the astrophysical environments, such as $^{12}C + ^{12}C$ and $^{16}O + ^{16}O$ fusion reactions.

The rest of paper is organized as follows. In Sec. II, we describe the theoretical framework of CC model and the

*Corresponding author: cxu@nju.edu.cn

construction process of Pauli blocking potential in $n\alpha$-nucleus-induced fusion reactions. In Sec. III, the total potentials and calculated fusion cross sections are compared. The density dependence of the Pauli blocking effects is analyzed. The summary is displayed in Sec. IV.

II. THEORETICAL FRAMEWORK

We apply the CCFULL code to calculate the fusion cross sections [10,37]. In the calculations, the incoming wave boundary condition (IWBC) is imposed and the absorption radius is taken to be at the minimum of the potential inside the Coulomb barrier [10,37]. With the IWBC, the coupled-channels equations can be given by [10]

$$\left[-\frac{\hbar^2}{2\mu}\frac{d^2}{dR^2}+\frac{J(J+1)\hbar^2}{2\mu R^2}+V(R)+\epsilon_n-E\right]u_n(R)+\sum_m V_{nm}(R)u_m(R)=0, \quad (1)$$

where E is the incident energy in the center-of-mass frame, ϵ_n is the excitation energy of the nth channel, and u_n is the radial wave function of the nth channel. The total potential $V(R)$ between two colliding nuclei consists of both Coulomb and nuclear interactions, i.e., $V(R)=V_N(R)+V_C(R)$. The nuclear interaction $V_N(R)$ and Coulomb interaction $V_C(R)$ used in calculations are obtained by double folding procedure.

The symbol $V_{nm}(R)$ in Eq. (1) denotes the matrix of coupling Hamiltonian which includes both the Coulomb and nuclear components. The Coulomb coupling matrix elements V^C_{nm} are calculated by the linear coupling approximation [10,37,38]. The nuclear coupling Hamiltonian is generated by introducing a dynamical operator $\hat{O}_\lambda$ in the calculations and given by $\widetilde{V}_N(R,\hat{O}_\lambda)=V_N(R-\hat{O}_\lambda)$ [10,37]. For the vibrational coupling, the operator $\hat{O}_\lambda$ is given by $\hat{O}_\lambda=(\beta^*/\sqrt{4\pi})R_i(\alpha^\dagger_{\lambda 0}+\alpha_{\lambda 0})$ [10,37,38], where $\alpha^\dagger_{\lambda 0}$ and $\alpha_{\lambda 0}$ are the creation and annihilation operators of the phonons, respectively, the eigenvalues λ and eigenvectors $|\alpha\rangle$ of the operator $\hat{O}$ satisfy $\hat{O}_\lambda|\alpha\rangle=\lambda_\alpha|\alpha\rangle$, R_i is the radius of the projectile or target, and β^* denotes the corresponding deformation parameter. The nuclear coupling matrix elements are then evaluated by [10,37,38]

$$V^N_{nm}=\langle n|\widetilde{V}_N(R,\hat{O}_\lambda)|m\rangle-V_N(R)\delta_{n,m}=\sum_\alpha\langle n|\alpha\rangle\langle\alpha|m\rangle\widetilde{V}_N(R,\lambda_\alpha)-V_N(R)\delta_{n,m}. \quad (2)$$

The nuclear coupling potential $\widetilde{V}_N(R,\lambda_\alpha)=V_N(R-\lambda_\alpha)$ is taken up to the second order of λ_α [10,37,38]

$$\widetilde{V}_N(R,\lambda_\alpha)=V_N(R)-\frac{dV_N(R)}{dR}\lambda_\alpha+\frac{1}{2}\frac{d^2V_N(R)}{dR^2}\lambda^2_\alpha, \quad (3)$$

where the first term $V_N(R)$ is the nuclear potential in the absence of the coupling, which consists of not only the direct term but also the Pauli blocking term $V^{n\alpha}_P(R)$ [see Eq. (5) below]. The second and third terms are the nuclear coupling form factor, which is closely associated with the nuclear potential. As a part of $V_N(R)$, the Pauli blocking potential $V^{n\alpha}_P(R)$ plays a nonnegligible role in the nuclear coupling matrix elements.

TABLE I. Parameters of the density distribution for ^{12}C, ^{16}O, ^{24}Mg, and ^{28}Si nuclei. The last column is the corresponding references from where the parameters are taken.

Nucleus	ρ_{0p} (fm^{-3})	ω (fm^{-2})	γ (fm^{-2})	Ref.
^{12}C	0.1644	0.4988	0.3741	[41]
^{16}O	0.1317	0.6457	0.3228	[41]
^{24}Mg	0.2161	0.1513	0.2186	[42]
^{28}Si	0.2052	0.1941	0.2112	[42]

By solving the CC equations the penetrability P_J can be obtained and the total fusion cross section $\sigma_{\rm fus}$ is then given by summing the partial fusion cross section [10]

$$\sigma_{\rm fus}(E)=\frac{\pi}{k^2}\sum_J(2J+1)P_J(E), \quad (4)$$

where $k=\sqrt{2\mu E/\hbar^2}$ is the wave number associated with the energy E.

Let us now discuss the explicit form of the potential between projectile and target. In addition to the attractive nuclear interaction and the repulsive Coulomb interaction, there is a nonnegligible Pauli repulsive interaction between two colliding nuclei. When the projectile and target nuclei start touching each other, the Pauli blocking effects become increasingly important due to the density overlap. To this end, a Pauli blocking potential, $V^{n\alpha}_P$, as the consequence of antisymmetrization, is introduced to replace the exchange term in the standard Michigan-3-Yukawa (M3Y) potential as follows:

$$V_N(\mathbf{R})=\int d\mathbf{r_1}d\mathbf{r_2}\rho_p(\mathbf{r_1})\rho_t(\mathbf{r_2})g(|\mathbf{s}|)+V^{n\alpha}_P(\mathbf{R}), \quad (5)$$

with

$$g(|\mathbf{s}|)=\left[c_1\frac{\exp(-4s)}{4s}-c_2\frac{\exp(-2.5s)}{2.5s}\right]F(\rho), \quad (6)$$

and

$$F(\rho)=C[1+\alpha\exp(-\beta\rho)]. \quad (7)$$

In Eq. (5), the symbol $\mathbf{R}$ denotes the distance between the center-of-mass of two colliding nuclei and the quantity $|\mathbf{s}|(\mathbf{s}=\mathbf{R}-\mathbf{r_1}+\mathbf{r_2})$ is the distance between a nucleon in the target and a nucleon in the projectile.

The density distribution of projectiles ρ_p employed in Eq. (5) is a modified Gaussian shape [39,40]

$$\rho_p(r)=\rho_{0p}(1+\omega r^2)\exp(-\gamma r^2), \quad (8)$$

where the parameters ω and γ are obtained by fitting the corresponding root-mean-square (rms) radii and ρ_{0p} is determined by integrating the density distribution equivalent to the corresponding mass number [41,42]. Their values used in calculations are listed in Table I.

The density distribution of target ρ_t adopted in Eq. (5) can be given by the standard Fermi form [43]

$$\rho_t(r)=\frac{\rho_{0t}}{1+\exp\left(\frac{r-c}{a}\right)}, \quad (9)$$

TABLE II. Parameters of the density distribution for ^{30}Si, ^{198}Pt, and ^{208}Pb target nuclei. The symbols c_p, a_p, c_n, and a_n denote the half-density radius and diffuseness parameters of proton and neutron in target nuclei. The last column is the corresponding references.

Nucleus	c_p (fm)	a_p (fm)	c_n (fm)	a_n (fm)	Ref.
^{30}Si	3.165	0.48	3.17	0.43	[44]
^{198}Pt	6.510	0.495	6.645	0.557	[45]
^{208}Pb	6.68	0.447	6.7	0.55	[46]

in which c and a are half-density radius and diffuseness parameters and ρ_{0t} is determined by the normalization condition. The values of c and a used in calculations are listed in Table II.

In what follows we focus attention on the construction of the Pauli blocking potential $V_P^{n\alpha}$ in Eq. (5). In our analysis, all projectile nuclei studied are assumed to be composed of α particles, i.e., the mass number of projectile $A = 4n$. The α clusters in these projectiles are regarded as the elementary units and the Pauli blocking potential of two colliding nuclei $V_P^{n\alpha}$ depends on the density distribution of both projectile and target.

The density distribution of α particle in projectile is the widely used Gaussian form [47–49]

$$\rho_\alpha(r) = \rho_{0\alpha} \exp(-\lambda r^2), \tag{10}$$

where the parameters are taken as $\rho_{0\alpha} = 0.4229$ fm^{-3} and $\lambda = 0.7024$ fm^{-2} from Ref. [47]. In order to relate the density distribution of projectile ρ_p to that of the α particle ρ_α, an α-cluster distribution function inside the nucleus, $\rho_c(r)$, was proposed to satisfy the condition in Ref. [39],

$$\rho_p(\mathbf{r}) = \int \rho_c(\mathbf{r}')\rho_\alpha(|\mathbf{r} - \mathbf{r}'|)d\mathbf{r}'. \tag{11}$$

By using the Fourier transform techniques [47], the α-cluster distribution function $\rho_c(r)$ can be given by [40]

$$\rho_c(r) = \rho_{0c}(1 + \mu r^2)\exp(-\xi r^2), \tag{12}$$

with

$$\eta = \lambda - \gamma, \quad \xi = \gamma\lambda/\eta, \quad \mu = \frac{2\omega\lambda^2}{\eta(2\eta - 3\omega)}, \tag{13}$$

where ρ_{0c} is obtained by integrating Eq. (11) equivalent to the mass number of projectiles.

Therefore, the Pauli blocking potential of $n\alpha$ nuclei in fusion reactions can be constructed by using a single folding procedure,

$$V_P^{n\alpha}(\mathbf{R}) = \int \rho_c(\mathbf{r}')V_p^\alpha(\mathbf{R} + \mathbf{r}')d\mathbf{r}', \tag{14}$$

in which V_p^α is the Pauli blocking potential of one α particle in nuclear matter. This microscopic Pauli blocking potential V_p^α is obtained by solving the in-medium four-nucleon wave equation with a variational approach and a good fit formula is given by [46,50,51]

$$V_P^\alpha(\rho_t) = 4515.9\rho_t - 100935\rho_t^2 + 1202538\rho_t^3. \tag{15}$$

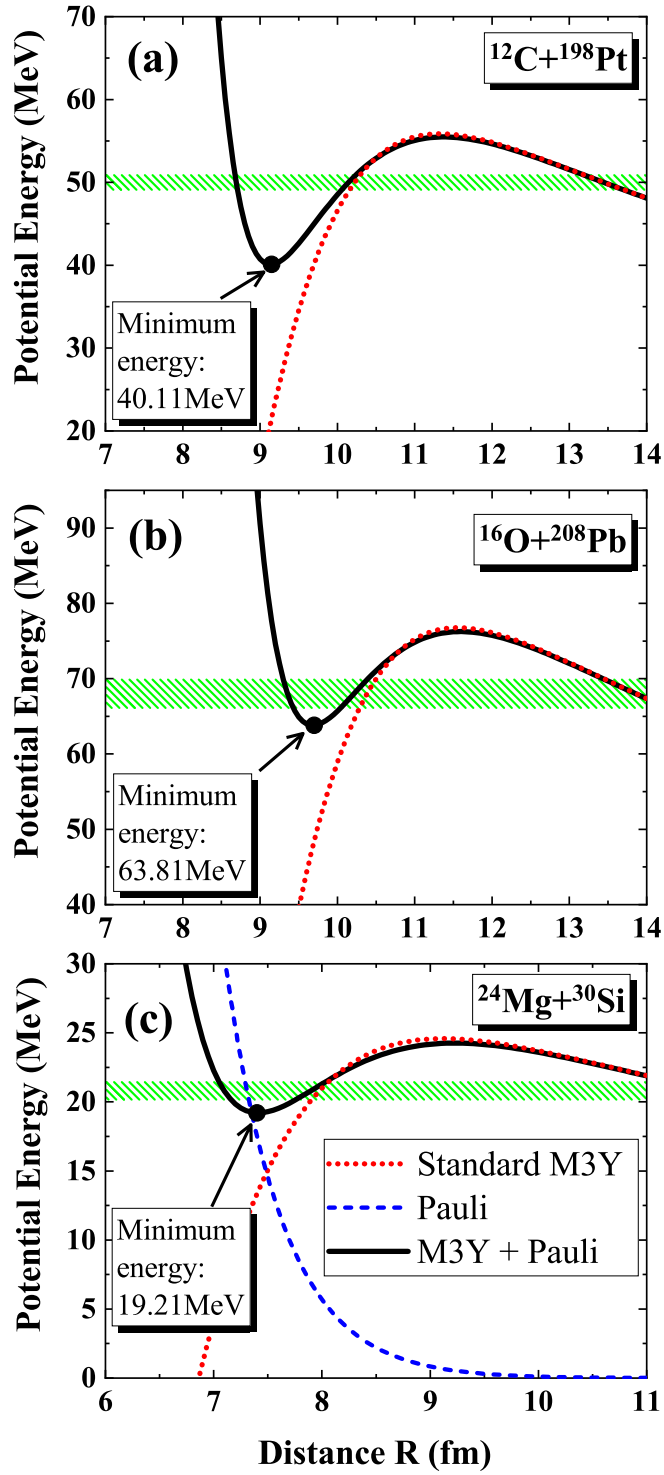

FIG. 1. Comparison of the total potentials obtained from standard M3Y nuclear interaction (dotted lines) with the one obtained from M3Y+ Pauli nuclear interaction (solid lines) for ^{12}C + ^{198}Pt, ^{16}O + ^{208}Pb, and ^{24}Mg + ^{30}Si fusion systems. The shadow region denotes the experimental threshold energy E_s of fusion hindrance [5–7]. The Pauli blocking interaction in ^{24}Mg + ^{30}Si is given by the dashed line in (c).

As a reverse quantum tunneling process with fusion, this Pauli blcking potential has been successfully applied into the

TABLE III. Parameters used in the CC calculations. The symbol λ^π denotes the multipolarity and the parity of a state. The symbol E_{ex} denotes the excitation energy of a state. The deformation parameter is denoted by symbol β^*. The symbol N_{ph} in the last column is the number of phonons included in the calculations.

Nucleus	λ^π	E_{ex} (MeV)	β^*	N_{ph}
(1) $^{12}C + ^{198}Pt$ (Refs. [5,53])				
^{12}C	2^+	4.44	0.59	1
^{198}Pt	2^+	0.407	0.11	1
	3^-	1.5	0.1	1
(2) $^{16}O + ^{208}Pb$ (Ref. [18])				
^{16}O	2^+	6.92	0.352	1
	3^-	6.13	0.713	1
^{198}Pb	3^-	2.615	0.111	1
	5^-	3.198	0.059	1
(3) $^{24}Mg + ^{30}Si$ (Ref. [7])				
^{24}Mg	2^+	1.369	0.608	1
^{30}Si	2^+	2.235	0.33	1
	3^-	5.488	0.275	1
(4) $^{28}Si + ^{30}Si$ (Ref. [7])				
^{30}Si	2^+	2.235	0.33	1
	3^-	5.488	0.275	1

radioactive α-cluster decay in heavy nuclei and superheavy nuclei [46,50,51]. For α-induced fusion reactions, the preliminary work shows this Pauli blocking potential also has a good adaptability [29].

Next we detail the parameters used in the direct part, $g(|\mathbf{s}|)$, of the density-dependent M3Y effective nucleon-nucleon interaction in Eq. (5). The symbols c_1 and c_2 in Eq. (6) are the strength of the Yukawa interactions and their fitted values are $c_1 = 2535$ MeV fm and $c_2 = 1563$ MeV fm, respectively. The density dependence of the nucleon-nucleon interaction adopted here is the CDM3Y1 interaction. The values of the density-dependent parameters C, α, and β in Eq. (7) are 0.3428, 3.0232, and 3.5512 fm^3, respectively [13,52]. The density ρ in Eq. (7) is defined as $\rho = \rho_p + \rho_t$.

III. RESULTS AND DISCUSSION

Taking the $^{12}C + ^{198}Pt$, $^{16}O + ^{208}Pb$, and $^{24}Mg + ^{30}Si$ fusion systems as examples, we first compare in Fig. 1 the total potentials constructed from the "M3Y + Pauli" nuclear interaction with the one constructed from the "standard M3Y" nuclear interaction. The parameters of density distribution of the projectiles and targets are listed in Tables I and II, respectively.

In Fig. 1, it is seen that the M3Y+ Pauli potential has a thicker barrier width than standard M3Y potential below the experimental threshold energy (shadow region), which is considered as the onset of energy in the fusion hindrance phenomenon [31]. More interestingly, a shallow pocket in the inner region of the Coulomb barrier is generated by the M3Y + Pauli potential, while there is a rapid decrease at short distance for the standard M3Y potential, in which the Pauli blocking effect after the density overlap of two colliding nuclei is not fully considered [13]. The minimum energy of this

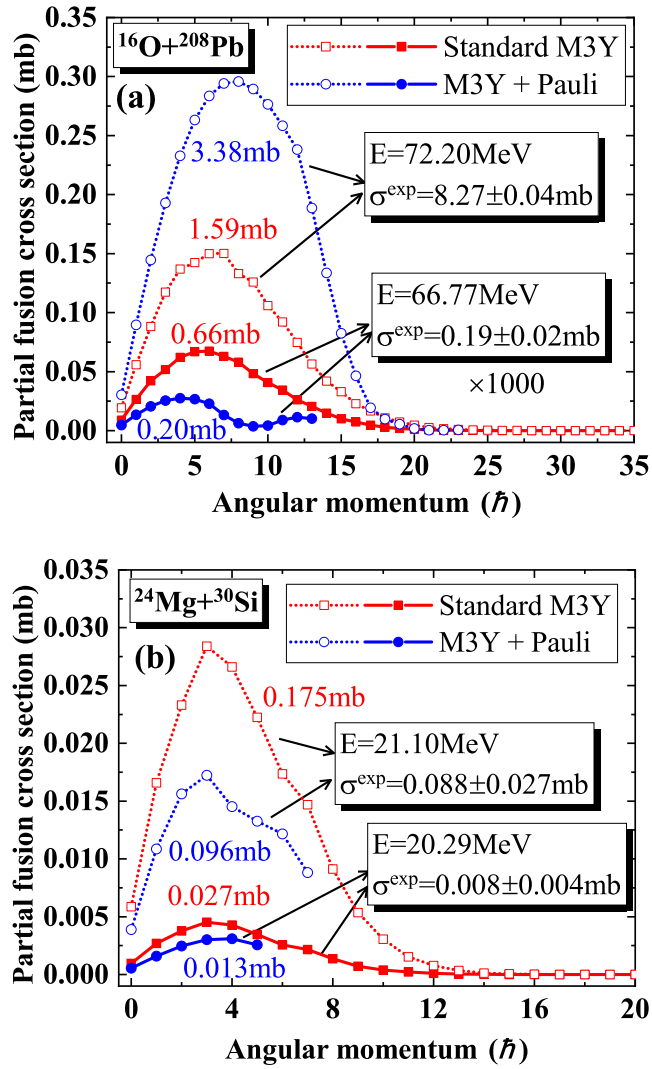

FIG. 2. The partial fusion cross sections calculated by standard M3Y potential (the solid lines with solid squares and the dotted lines with open squares) and M3Y + Pauli potential (the solid lines with solid circles and the dotted lines with open circles) at different colliding energies for (a) $^{16}O + ^{208}Pb$ and (b) $^{24}Mg + ^{30}Si$ fusion systems. Note that the results at $E = 66.77$ MeV for $^{16}O + ^{208}Pb$ system have been multiplied by 1000. The values of total fusion cross sections calculated by various potentials and the experimental data σ^{exp} [6,7,54] at specified colliding energies are given.

pocket for each system V_{min} is denoted by the solid circle. This energy determines the minimum energy of the occurrance of the fusion reaction in present model and below this energy, the calculated cross section will be zero. In addition, as shown in Fig. 1(c) the Pauli blocking potential $V_P^{n\alpha}$ for $^{24}Mg + ^{30}Si$ fusion system (denoted by the dashed line) becomes more and more important with the decrease of the distances between the centers of projectile and target. After a large distance ($R \geqslant 10$ fm), this Pauli blocking potential becomes very weak and could be neglected and two potentials have almost the same behavior in the outer region.

We incorporate the above two potentials in the computer code CCFULL [37] to calculate the fusion cross sections.

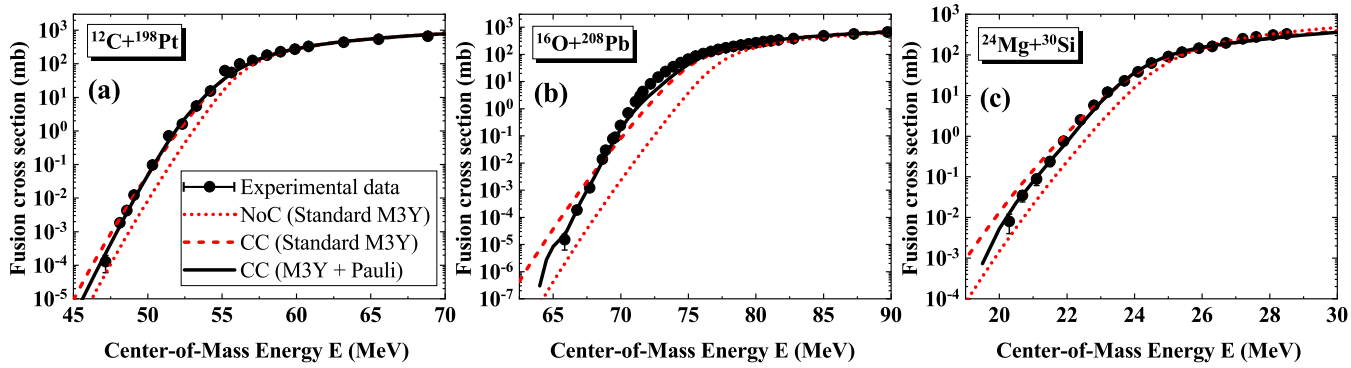

FIG. 3. The experimental fusion cross sections for $^{12}C + ^{198}Pt$ [5,55], $^{16}O + ^{208}Pb$ [6,54], and $^{24}Mg + ^{30}Si$ [7,56] fusion systems compared with the CC calculations obtained by standard M3Y potential (dashed lines) and M3Y + Pauli potential (solid lines). The dotted lines denote the no-coupling results for the standard M3Y potential.

Note that the potential between two nuclei is, of course, an important input in the CC calculation. Other inputting parameters for the coupling strengths are tabulated in Table III. In Fig. 2, we calculate the partial fusion cross sections as a function of the angular momentum and compare the total fusion cross sections with the experimental data $\sigma^{\rm exp}$ at several typical experimental colliding energies, namely, 72.20 MeV, 66.77 MeV for $^{16}O + ^{208}Pb$ [6,54] and 21.10 MeV, 20.29 MeV for $^{24}Mg + ^{30}Si$ [7]. The total fusion cross sections calculated by M3Y+ Pauli potential agree more closely with the experimental data than the results of standard M3Y potential. At deep subbarrier energies, such as 66.77 MeV for $^{16}O + ^{208}Pb$ and 21.10 and 20.29 MeV for $^{24}Mg + ^{30}Si$, the partial fusion cross sections have a significant reduction by considering the Pauli blocking effects as compared to the values calculated by standard M3Y potential. In addition, the maximum angular momentum calculated in M3Y + Pauli potential is much smaller than the one calculated in standard M3Y potential, i.e., the M3Y + Pauli potential prevents the penetration of high-order partial waves to the Coulomb barrier and results in a slight reduction of total fusion cross sections.

In Fig. 3, the total fusion cross sections calculated by M3Y + Pauli and standard M3Y potentials versus the colliding energies are compared with the experimental data for $^{12}C + ^{198}Pt$ [5,55], $^{16}O + ^{208}Pb$ [6,54], and $^{24}Mg + ^{30}Si$ [7,56] fusion systems. The dotted and dashed lines are the fusion cross sections calculated by the standard M3Y potential without and with the CC effects, respectively. The solid lines denote the results obtained from the M3Y + Pauli potential with the CC effects. By taking into account the Pauli blocking effects, the fusion cross sections obtained from M3Y + Pauli potential are in agreement with the experimental data, while the results calculated by standard M3Y potential overestimate the experimental data at deep subbarrier energies. Note that in Figs. 3(b) and 3(c), the calculated cross sections vanish at the center-of-mass energies $E < V_{\rm min}$ (63.81 MeV for $^{16}O + ^{208}Pb$ and 19.21 MeV for $^{24}Mg + ^{30}Si$) as mentioned above.

To further study the density dependence of the Pauli blocking effects, we compare the fusion processes of the different projectiles ^{12}C, ^{24}Mg, and ^{28}Si with the same target ^{30}Si in Fig. 4. The parameters used in CC calculations for $^{28}Si + ^{30}Si$ system are listed in Table III and the calculated fusion cross sections of $^{12}C + ^{30}Si$ system result from the one-dimensional potential model. Figure 4 shows that the fusion cross sections calculated by M3Y + Pauli potential for $^{12}C + ^{30}Si$ [4], $^{24}Mg + ^{30}Si$ [7,56], and $^{28}Si + ^{30}Si$ [8] fusion systems are in agreement with the experimental data. The insert shows the Pauli blocking potential verses the density of target ^{30}Si for corresponding fusion systems. As expected, the heavier projectiles, namely ^{24}Mg and ^{28}Si, are subjected to the stronger Pauli blocking effects in target ^{30}Si than projectile ^{12}C. Moreover, the Pauli blocking potentials in relatively heavy-mass fusion systems $^{24}Mg + ^{30}Si$ and $^{28}Si + ^{30}Si$ increase rapidly with the increasing of the target density, while a slow increasing is shown in light-mass fusion system $^{12}C + ^{30}Si$. This result indicates the fusion hindrance becomes gradually obvious in moving from the lighter (^{12}C) to the

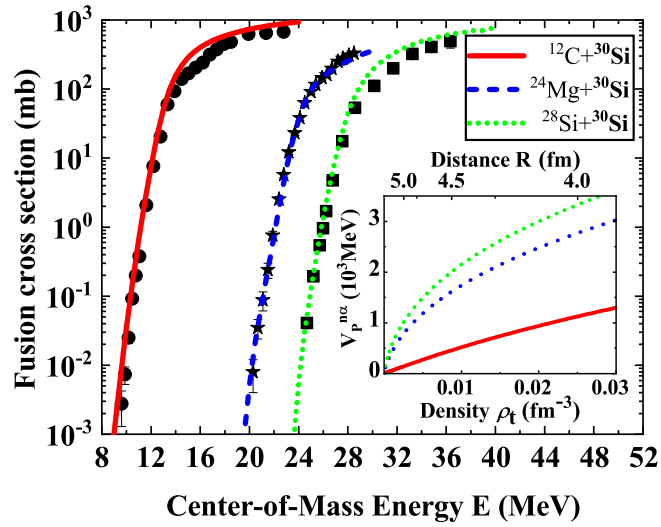

FIG. 4. The experimental fusion cross sections for $^{12}C + ^{30}Si$ [4], $^{24}Mg + ^{30}Si$ [7,56], and $^{28}Si + ^{30}Si$ [8] fusion systems compared with the results calculated by M3Y + Pauli potential. The Pauli blocking potentials versus the density of target are given in the insert, in which the bottom horizontal axis ρ_t is the matter density of ^{30}Si and the top horizontal axis R is the corresponding internuclear distance.

heavier projectiles (^{24}Mg and ^{28}Si) with the same target (^{30}Si) and a similar phenomenon is also found in the experimental fusion cross sections of ^{6,7}Li, ^{12}C + ^{198}Pt by Shrivastava *et al.* [5].

IV. SUMMARY

Based on the Pauli blocking term obtained from the finite-temperature Green function approach [57], a Pauli blocking potential is constructed in the $n\alpha$-nucleus-induced fusion reactions by using a single folding procedure, in which the $n\alpha$-nuclei are assumed to be consisted of α particles and can be described by an α-cluster distribution function. By introducing this Pauli blocking potential, it is found there exists a shallow pocket in the potentials of ^{12}C + ^{198}Pt, ^{16}O + ^{208}Pb, and ^{24}Mg + ^{30}Si fusion systems.

For fusion systems ^{16}O + ^{208}Pb and ^{24}Mg + ^{30}Si, it is found that, at deep subbarrier energies, the partial fusion cross sections calculated by considering the Pauli blocking effects are much smaller than the ones calculated by standard M3Y potential and the high-angular-momentum partial waves in fusion process are shielded by the potential with a shallow pocket. The fusion hindrances in ^{12}C + ^{198}Pt, ^{16}O + ^{208}Pb, ^{12}C + ^{30}Si, ^{24}Mg + ^{30}Si, and ^{28}Si + ^{30}Si systems at deep subbarrier energies are described well by using the M3Y + Pauli potential.

By comparing the Pauli blocking effects in different projectiles ^{12}C, ^{24}Mg, and ^{28}Si with the same target ^{30}Si, it is found that the Pauli blocking potentials in the heavier projectiles ^{24}Mg and ^{28}Si have a rapid increase along with the density of target ^{30}Si, while a gentle increasing is shown in lighter projectile ^{12}C. This, to some extent, can be helpful to understanding the fusion process at astrophysical energies for light fusion systems, such as ^{12}C + ^{12}C and ^{16}O + ^{16}O reactions.

ACKNOWLEDGMENTS

This work is supported by the National Natural Science Foundation of China (Grants No. 11822503 and No. 11575082) and by the Fundamental Research Funds for the Central Universities (Nanjing University).

[1] C. L. Jiang, H. Esbensen, K. E. Rehm, B. B. Back, R. V. F. Janssens, J. A. Caggiano, P. Collon, J. Greene, A. M. Heinz, D. J. Henderson, I. Nishinaka, T. O. Pennington, and D. Seweryniak, Phys. Rev. Lett. **89**, 052701 (2002).
[2] C. L. Jiang, K. E. Rehm, R. V. F. Janssens, H. Esbensen, I. Ahmad, B. B. Back, P. Collon, C. N. Davids, J. P. Greene, D. J. Henderson, G. Mukherjee, R. C. Pardo, M. Paul, T. O. Pennington, D. Seweryniak, S. Sinha, and Z. Zhou, Phys. Rev. Lett. **93**, 012701 (2004).
[3] C. L. Jiang, B. B. Back, H. Esbensen, R. V. F. Janssens, Ş. Mişicu, K. E. Rehm, P. Collon, C. N. Davids, J. P. Greene, D. J. Henderson, L. Jisonna, S. Kurtz, C. J. Lister, M. Notani, M. Paul, R. Pardo, D. Peterson, D. Seweryniak, B. Shumard, X. D. Tang, I. Tanihata, X. Wang, and S. Zhu, Phys. Lett. B **640**, 18 (2006).
[4] G. Montagnoli, A. M. Stefanini, C. L. Jiang, K. Hagino, F. Galtarossa, G. Colucci, S. Bottoni, C. Broggini, A. Caciolli, P. Čolović, L. Corradi, S. Courtin, R. Depalo, E. Fioretto, G. Fruet, A. Gal, A. Goasduff, M. Heine, S. P. Hu, M. Kaur, T. Mijatović, M. Mazzocco, D. Montanari, F. Scarlassara, E. Strano, S. Szilner, and G. X. Zhang, Phys. Rev. C **97**, 024610 (2018).
[5] A. Shrivastava, K. Mahata, S. K. Pandit, V. Nanal, T. Ichikawa, K. Hagino, A. Navin, C. S. Palshetkar, V. V. Parkar, K. Ramachandran, P. C. Rout, Abhinav Kumar, A. Chatterjee, and S. Kailas, Phys. Lett. B **755**, 332 (2016).
[6] M. Dasgupta, D. J. Hinde, A. Diaz-Torres, B. Bouriquet, Catherine I. Low, G. J. Milburn, and J. O. Newton, Phys. Rev. Lett. **99**, 192701 (2007).
[7] C. L. Jiang, A. M. Stefanini, H. Esbensen, K. E. Rehm, S. Almaraz-Calderon, B. B. Back, L. Corradi, E. Fioretto, G. Montagnoli, F. Scarlassara, D. Montanari, S. Courtin, D. Bourgin, F. Haas, A. Goasduff, S. Szilner, and T. Mijatovic, Phys. Rev. Lett. **113**, 022701 (2014).
[8] C. L. Jiang, B. B. Back, H. Esbensen, J. P. Greene, R. V. F. Janssens, D. J. Henderson, H. Y. Lee, C. J. Lister, M. Notani, R. C. Pardo, N. Patel, K. E. Rehm, D. Seweryniak, B. Shumard, X. Wang, S. Zhu, S. Mişicu, P. Collon, and X. D. Tang, Phys. Rev. C **78**, 017601 (2008).
[9] A. B. Balantekin and N. Takigawa, Rev. Mod. Phys. **70**, 77 (1998).
[10] K. Hagino and N. Takigawa, Prog. Theor. Phys. **128**, 1061 (2012).
[11] K. Hagino, N. Rowley, and M. Dasgupta, Phys. Rev. C **67**, 054603 (2003).
[12] K. Washiyama, K. Hagino, and M. Dasgupta, Phys. Rev. C **73**, 034607 (2006).
[13] I. I. Gontchar, D. J. Hinde, M. Dasgupta, and J. O. Newton, Phys. Rev. C **69**, 024610 (2004).
[14] J. O. Newton, R. D. Butt, M. Dasgupta, D. J. Hinde, I. I. Gontchar, C. R. Morton, and K. Hagino, Phys. Rev. C **70**, 024605 (2004).
[15] C. J. Lin, Phys. Rev. Lett. **91**, 229201 (2003).
[16] Ş. Mişicu and H. Esbensen, Phys. Rev. Lett. **96**, 112701 (2006).
[17] Ş. Mişicu and H. Esbensen, Phys. Rev. C **75**, 034606 (2007).
[18] H. Esbensen and Ş. Mişicu, Phys. Rev. C **76**, 054609 (2007).
[19] T. Ichikawa, K. Hagino, and A. Iwamoto, Phys. Rev. C **75**, 064612 (2007).
[20] T. Ichikawa, K. Hagino, and A. Iwamoto, Phys. Rev. Lett. **103**, 202701 (2009).
[21] T. Ichikawa, Phys. Rev. C **92**, 064604 (2015).
[22] K. Hagino and Y. Watanabe, Phys. Rev. C **76**, 021601(R) (2007).
[23] A. Diaz-Torres, D. J. Hinde, M. Dasgupta, G. J. Milburn, and J. A. Tostevin, Phys. Rev. C **78**, 064604 (2008).
[24] A. S. Umar and V. E. Oberacker, Phys. Rev. C **74**, 021601(R) (2006).
[25] A. S. Umar, C. Simenel, and V. E. Oberacker, Phys. Rev. C **89**, 034611 (2014).
[26] V. Yu. Denisov, Phys. Rev. C **89**, 044604 (2014).
[27] V. Yu. Denisov, Phys. Rev. C **91**, 024603 (2015).
[28] E. Uegaki and Y. Abe, Prog. Theor. Phys. **90**, 615 (1993).

[29] K. Cheng and C. Xu, Phys. Rev. C **99**, 014607 (2019).
[30] B. B. Back, H. Esbensen, C. L. Jiang, and K. E. Rehm, Rev. Mod. Phys. **86**, 317 (2014).
[31] C. L. Jiang, K. E. Rehm, B. B. Back, and R. V. F. Janssens, Phys. Rev. C **79**, 044601 (2009).
[32] K. Wildermuth and Y. C. Tang, *A Unified Theory of the Nucleus* (Vieweg, Braunschweig, Germany, 1977).
[33] G. F. Bertsch and W. Bertozzi, Nucl. Phys. A **165**, 199 (1971).
[34] Y. Fujiwara, H. Horiuchi, K. Ikeda, M. Kamimura, K. Kato, Y. Suzuki, and E. Uegaki, Prog. Theor. Phys. Suppl. **68**, 29 (1980).
[35] A. Tohsaki, H. Horiuchi, P. Schuck, and G. Röpke, Phys. Rev. Lett. **87**, 192501 (2001).
[36] J. A. Maruhn, M. Kimura, S. Schramm, P. G. Reinhard, H. Horiuchi, and A. Tohsaki, Phys. Rev. C **74**, 044311 (2006).
[37] K. Hagino, N. Rowley, and A. T. Kruppa, Comput. Phys. Commun. **123**, 143 (1999).
[38] H. Esbensen and S. Landowne, Phys. Rev. C **35**, 2090 (1987).
[39] M. El-Azab Farid, Z. M. M. Mahmoud, G. S. Hassan, Nucl. Phys. A **691**, 671 (2001).
[40] G. Kocak, M. Karakoc, I. Boztosun, and A. B. Balantekin, Phys. Rev. C **81**, 024615 (2010).
[41] S. Qint-biao, F. Da-chun, and Z. Yi-zhong, Phys. Rev. C **43**, 2773 (1991).
[42] O. M. Knyazkov and E. F. Hefter, Z. Phys. A **301**, 277 (1981).
[43] A. Bohr and B. R. Mottelson, *Nuclear Structure*, Vol. 1 (World Scientific, Singapore, 1998).
[44] G. Colucci, G. Montagnoli, A. M. Stefanini, H. Esbensen, D. Bourgin, P. Čolović, L. Corradi, M. Faggian, E. Fioretto, F. Galtarossa, A. Goasduff, J. Grebosz, F. Haas, M. Mazzocco, F. Scarlassara, C. Stefanini, E. Strano, S. Szilner, M. Urbani, and G. L. Zhang, Phys. Rev. C **97**, 044613 (2018).
[45] W. M. Seif and H. Mansour, Int. J. Mod. Phys. E **24**, 1550083 (2015).
[46] C. Xu, G. Röpke, P. Schuck, Z. Ren, Y. Funaki, H. Horiuchi, A. Tohsaki, T. Yamada, and B. Zhou, Phys. Rev. C **95**, 061306(R) (2017).
[47] G. R. Satchler and W. G. Love, Phys. Rep. **55**, 183 (1979).
[48] C. Xu and Z. Ren, Phys. Rev. C **74**, 014304 (2006).
[49] J. Fan and C. Xu, Nucl. Phys. A **989**, 1 (2019).
[50] G. Röpke, P. Schuck, Y. Funaki, H. Horiuchi, Z. Ren, A. Tohsaki, C. Xu, T. Yamada, and B. Zhou, Phys. Rev. C **90**, 034304 (2014).
[51] C. Xu, Z. Ren, G. Röpke, P. Schuck, Y. Funaki, H. Horiuchi, A. Tohsaki, T. Yamada, and B. Zhou, Phys. Rev. C **93**, 011306(R) (2016).
[52] D. T. Khoa, G. R. Satchler, and W. von Oertzen, Phys. Rev. C **56**, 954 (1997).
[53] A. Shrivastava, A. Navin, A. Diza-Torres, V. Nanal, K. Ramachandran, M. Rejmund, S. Bhattacharyya, A. Chatterjee, S. Kailas, A. Lemasson, R. Palit, V. V. Parkar, R. G. Pillay, P. C. Rout, and Y. Sawant, Phys. Lett. B **718**, 931 (2013).
[54] C. R. Morton, A. C. Berriman, M. Dasgupta, D. J. Hinde, J. O. Newton, K. Hagino, and I. J. Thompson, Phys. Rev. C **60**, 044608 (1999).
[55] A. Shrivastava, S. Kailas, A. Chatterjee, A. Navin, A. M. Samant, P. Singh, S. Santra, K. Mahata, B. S. Tomar, and G. Pollarolo, Phys. Rev. C **63**, 054602 (2001).
[56] A. Morsad, J. J. Kolata, R. J. Tighe, X. J. Kong, E. F. Aguilera, and J. J. Vega, Phys. Rev. C **41**, 988 (1990).
[57] G. Röpke, Phys. Rev. C **79**, 014002 (2009).